Available online at www.sciencedirect.com

ScienceDirect

Mendeleev Commun., 2022, **32**, 520–522

Mendeleev Communications

Nanocomposite thin film structures based on polyarylenephthalide with SWCNT and graphene oxide fillers

Renat B. Salikhov,*[a] Rufina A. Zilberg,[b] Ilnur N. Mullagaliev,[a] Timur R. Salikhov[a] and Yulia B. Teres[b]

[a] *Institute of Physics and Technology, Bashkir State University, 450076 Ufa, Russian Federation. E-mail: salikhovrb@yandex.ru*

[b] *Department of Chemistry, Bashkir State University, 450076 Ufa, Russian Federation*

DOI: 10.1016/j.mencom.2022.07.029

Investigations of nanocomposite thin films based on polyarylenephthalide, single-walled carbon nanotubes and graphene oxide have been carried out. Using these films as a transport layer, field-effect transistors were assembled and their output and transfer characteristics were measured. The mobility of charge carriers was estimated and the obtained values are as follows: $\mu_{PAP/GO}$ = 0.020 cm^2 V^{-1} s^{-1} and $\mu_{PAP/SWCNT}$ = 0.071 cm^2 V^{-1} s^{-1}.

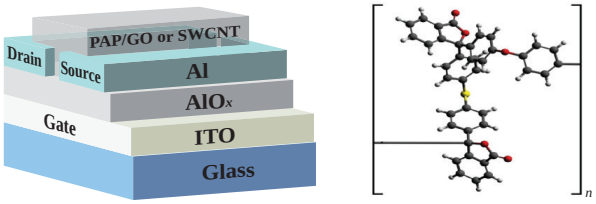

Keywords: thin films, polyarylenephthalide, carbon nanotubes, graphene oxide, voltammetry, impedance, field-effect transistor, composite sensors, charge carrier mobility.

Progress in polymer chemistry and nanotechnology stimulates the intensive development of organic electronics. Sustained interest is naturally directed to multifunctional compounds with electrically conductive, magnetic and optoelectronic properties.[1–3] Thin films of polyarylenephthalides (PAP) exhibit unique properties.[4–6] Among extremely promising materials for nanoelectronic devices, nanocomposite structures based on PAP, carbon nanotubes and graphene oxide (GO) should be singled out. These structures can be used to create elements and devices of molecular and polymer nanoelectronics, such as field-effect transistors and electrochemical sensors.

The use of functional nanomaterials, especially nanocomposite materials, is promising due to the larger electrode size, surface area, improved electrical conductivity of the sensor layer and chemical availability of the analyte.[7–9] These improvements are mainly due to the larger surface area, which facilitates access of the analyte to the electrode surface and thus favors the creation of highly sensitive sensor platforms. It is recognized that the potential of nanocomposites reinforced with nanostructured carbon materials opens up huge opportunities for their application in the 21st century.[10]

Studying the characteristics of the initial nanocomposite material before its use in electrochemical analysis is a necessary condition for the creation of efficient sensor platforms with improved electroanalytical parameters. There are numerous examples where nanomaterials such as multi-walled and single-walled carbon nanotubes (SWCNT), graphene, fullerenes and nanofibers dispersed into a polymer matrix have led to important advances in analytical electrochemistry, especially in the development of sensor devices.[11–17]

Of the polymer materials used to modify electrodes, PAP has successfully proven itself.[18–21] PAP films are electrically conductive, thermally stable, resistant to water, acids and alkalis, moreover they are soluble in many organic solvents. Based on them, enantioselective voltammetric sensors have been developed, for example, multisensor systems of the 'electronic tongue' type, in which each sensor is simultaneously sensitive to several components of the test solution, while the selectivity and sensitivity of the response to one or another detected component are different for different sensors (cross sensitivity).[18] Using a set of sensors, it is possible to simultaneously determine the concentrations of many or all components according to a predetermined complex multi-parameter relationship (multidimensional calibration). In particular, such systems are used for the recognition of medicines,[19] their enantiopurity[20] and medicine manufacturers.[21]

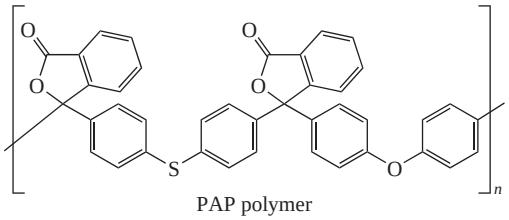

PAP polymer

PAP is a polymer with arylene fragments and heteroatoms in the main chain and carded phthalide groups. To create nanocomposite thin film structures, a polymer with the 1 : 1 ratio of oxydiphenylene and thiodiphenylene fragments was used.[22–25] To increase the electrical conductivity, effective surface area and sensor sensitivity, the PAP film was modified with SWCNT and GO (for experimental details, see Online Supplementary Materials).

Samples of field-effect transistors were fabricated from composites of PAP with GO and SWCNT (Figure 1) on glass substrates coated with ITO layers acting as a gate. Before the deposition of dielectric films, the substrates were annealed in a furnace at a temperature of 350 °C. AlO_x films with a thickness of 300 nm as a dielectric were deposited from solution by spin coating at 2000 rpm for 30 s and annealing in an oven at 350 °C for 1 h. Two aluminum electrodes, drain and source, 500 nm thick, were placed over the gate dielectric. A layer of semiconductor material of two types, either PAP/GO or PAP/SWCNT in another

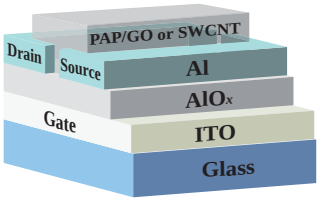

Figure 1 The structure of the experimental field-effect transistor.

version, was applied on the gap region by spin coating. The gap between the drain and source contacts was 50 μm, and the gap length was 2 mm.

To study the electrochemical properties of modified glassy carbon electrodes (GCE), such as GCE/PAP, GCE/PAP/GO and GCE/PAP/SWCNT, cyclic voltammetric and impedance measurements were carried out using an equimolar mixture of potassium hexacyanoferrates (II, III) as a redox standard. Cyclic voltammograms (CVs) correspond to a typical one-electron reversible redox process of the $[Fe(CN)_6]^{4-/3-}$ redox couple [Figure 2(*a*)]. CVs display that the incorporation of SWCNT and GO into the PAP film leads to an increase in the peak currents of the $[Fe(CN)_6]^{4-/3-}$ redox couple compared to the GCE/PAP electrode due to a decrease in the charge transfer resistance.

The Nernst value (ΔE) of the potential difference between the peak currents of oxidation and reduction for some modified electrodes can be very different from the usual value of ~60 mV when modifiers of a certain nature are used. For example, a noticeable deviation of this value (220 mV) has been reported[26] when using Nafion-modified electrodes. A similar deviation was also observed when using PAP-modified sensors or the PAP/CD system.[20] This deviation is explained[26] by the possible slowdown in the process kinetics due to the mutual repulsion of $[Fe(CN)_6]^{3-}$ and sulfo groups in the Nafion structure. In our case, a similar effect occurs, apparently, due to the repulsion of aromatic fragments of modifiers that are part of the GCE/PAP, GCE/PAP/GO and GCE/PAP/SWCNT electrodes and $[Fe(CN)_6]^{3-}$ anions. At the same time, modifiers containing GO and SWCNT lead to a greater deviation of ΔE from 60 mV. It should be noted that the deviation is more pronounced for the cathodic reaction than for the anodic one. This, apparently, is explained by a more pronounced repulsion between $[Fe(CN)_6]^{3-}$ and aromatic fragments of modifiers due to an increase in the electron density of the latter upon polarization at the cathode.

The electron transfer parameters were estimated by electrochemical impedance spectroscopy. Electrochemical impedance spectroscopy is widely used to analyze the complex electrical resistance of a system and is sensitive to surface phenomena and volume changes. A Randles equivalent circuit, consisting of electrolyte resistance (R_s), charge transfer resistance (R_{et}), Warburg impedance (W) and constant phase element (C_{dl}), was used to quantify the impedance data. The results obtained are presented in Table 1. Figure 2(*b*) shows the corresponding Nyquist plots. The semicircle in the high frequency region corresponds to the

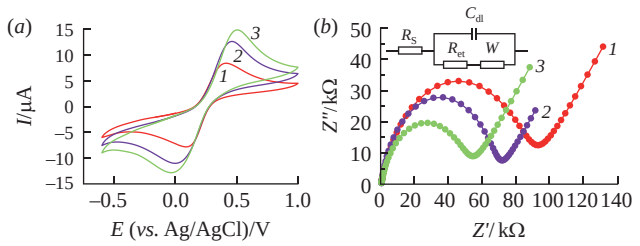

Figure 2 (*a*) CV curves of 5.0 mM $[Fe(CN)_6]^{4-/3-}$ (1:1) redox couple for (*1*) GCE/PAP, (*2*) GCE/PAP/GO and (*3*) GCE/PAP/SWCNT electrodes in 0.1 M KCl solution as supporting electrolyte at 100 mV s^{-1}. (*b*) Nyquist plots for the above electrodes in the presence of 5.0 mM $[Fe(CN)_6]^{4-/3-}$. Inset: Randles equivalent circuit used to simulate impedance data.

Table 1 Parameters of electrochemical impedance spectra and effective surface area according to CVs of the GCE/PAP, GCE/PAP/GO and GCE/PAP/SWCNT electrodes in the presence of 5.0 mM $[Fe(CN)_6]^{4-/3-}$ (n = 5, P = 0.95).

Electrode	A/mm^2	R_s/Ω	R_{et}/kΩ	C_{dl}/μS	W/μS
GCE/PAP	1.60 ± 0.06	497.0 ± 5.0	88.4 ± 4.1	0.05 ± 0.01	20.4 ± 0.3
GCE/PAP/GO	1.99 ± 0.08	495.3 ± 3.9	68.0 ± 0.7	0.06 ± 0.01	38.1 ± 1.0
GCE/PAP/SWCNT	2.42 ± 0.08	433.4 ± 2.2	51.2 ± 2.5	0.08 ± 0.03	24.0 ± 0.7

limiting stage of charge transfer. The rectilinear section for modified electrodes in the lower frequency region describes the diffusion component of charge transfer.[27] Nyquist plots [see Figure 2(*b*)] indicate that the GCE modified with PAP film has a higher charge transfer resistance than composite sensors, indicating that SWCNT and GO dispersed in PAP are materials with good conductivity[10,11] and, as a result, the electron transfer rate increases. It was noted that the addition of SWCNT to the composite is more efficient than the addition of GO. The constant phase element C_{dl} for electrodes modified with PAP and electrodes modified with PAP/GO or PAP/SWCNT composites changes insignificantly. The results obtained confirm the effectiveness of the proposed modification of the GCE.

The effective surface area of the electrodes under study (Table 1) was calculated according to the Randles–Ševčik equation

$$I_p = (2.69 \times 10^5) n^{3/2} A D^{1/2} c \nu^{1/2}, \quad (1)$$

where I_p is the oxidation peak current in A, n is the number of transferred electrons (n = 1), A is the electrode area in cm^2, D is the diffusion coefficient ($D = 7.6 \times 10^{-6}$ cm^2 s^{-1}), c is the concentration of $[Fe(CN)_6]^{4-/3-}$ in mM, and v is the scanning rate (v = 0.1 V s^{-1}).[28]

Studies have shown that composite sensors GCE/PAP/GO and GCE/PAP/SWCNT are characterized by an increase in the electron transfer rate and effective surface area compared to a sensor modified only with PAP, which allows them to be used subsequently in the electroanalysis of compounds of various nature, as well as for manufacturing field-effect transistors.

The morphology of the film surfaces was also studied using atomic force microscopy (Figure S1, see Online Supplementary Materials). The Gwyddion program was used to calculate the RMS roughness of the film surfaces over an area of 20 × 20 μm, which gave *Sq* values of 3, 42 and 221 nm for pure PAP, PAP/GO and PAP/SWCNT films, respectively. The obtained roughness values correspond to the effective surface area values given above.

The current–voltage characteristics (Figures 3 and 4) of the field-effect transistors were determined using a measurement scheme with a common source in open air at room temperature.

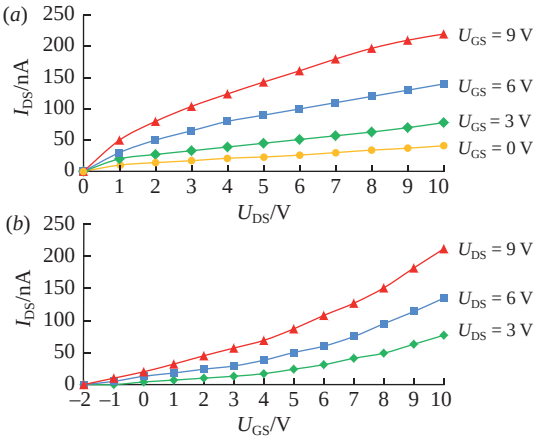

Figure 3 (*a*) Output and (*b*) transfer characteristics of a field-effect transistor with an active layer of PAP/GO.

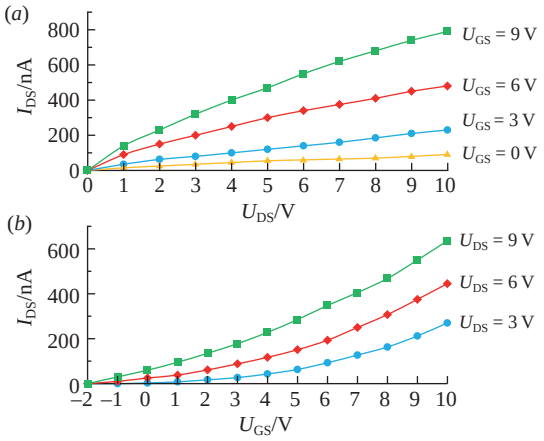

Figure 4 (*a*) Output and (*b*) transfer characteristics of a field-effect transistor with an active layer of PAP/SWCNT.

The output current is controlled at a positive gate bias, which indicates the electronic type of conductivity of the studied nanocomposite films. In the case of PAP films without GO and SWCNT additives, the low conductivity of the films does not allow obtaining the transistor effect.

The mobility of charge carriers of the resulting field-effect transistors was determined by the equation

$$I_{DS} = (W/L)\mu C(U_G - U_{th})U_{DS}, \quad (2)$$

where W is the channel width, L is the channel length, C is the capacitance per square area of the AlO_x gate dielectric (for a thickness of 500 nm, C = 7.1 nF cm^{-2}), U_G is the gate voltage, U_{DS} is the drain-to-source voltage, and U_{th} is the threshold voltage. The calculation showed that the mobility of charge carriers has the following values: $\mu_{PAP/GO}$ = 0.020 cm^2 V^{-1} s^{-1}, $\mu_{PAP/SWCNT}$ = 0.071 cm^2 V^{-1} s^{-1}. The error in the calculated values was about 10%. These mobility values were 3–4 orders of magnitude higher than the mobility values obtained for PAP films.[29] In our studies, the mobility values for PAP/GO and PAP/SWCNT composites are two times higher and an order of magnitude lower, respectively, than the previously reported values.[30,31]

The slope of the current–voltage characteristic was determined at ΔU from U = 4 V to U = 10 V and the corresponding currents. It was found that for a field-effect transistor based on PAP/GO it was K = 24, and for a transistor based on PAP/SWCNT K = 68. Thus, a stronger influence of the control voltage was found in transistors with a PAP/SWCNT transport layer.

Using the methods of cyclic voltammetry and electrochemical impedance spectroscopy, it has been found that composite sensors have a larger effective surface area and electron transfer rate compared to a sensor modified only with PAP, which allows them to be further used in the electroanalysis of substances of various nature.

We fabricated field-effect transistors using the studied PAP-based thin films as a transport layer and measured their output and transfer characteristics. The mobility of charge carriers was estimated and the following values were obtained: $\mu_{PAP/GO}$ = 0.020 cm^2 V^{-1} s^{-1} and $\mu_{PAP/SWCNT}$ = 0.071 cm^2 V^{-1} s^{-1}.

This work was supported by the Russian Science Foundation (grant no. 21-13-00169, https://rscf.ru/project/21-13-00169/) and the State assignment for the implementation of scientific research by laboratories (order MN-8/1356 of 09/20/2021).

Online Supplementary Materials

Supplementary data associated with this article can be found in the online version at doi: 10.1016/j.mencom.2022.07.029.

References

1 Z. Tao, T. Mohammed-Brahim, W. Lei, M. Harnois and E. Jacques, *Solid-State Electron.*, 2018, **150**, 51.
2 P. A. Shaposhnik, S. A. Zapunidi, M. V. Shestakov, E. V. Agina and S. A. Ponomarenko, *Russ. Chem. Rev.*, 2020, **89**, 1483.
3 M. Kang, A.-N. Cha, S.-A. Lee, S.-K. Lee, S. Bae, D.-Y. Jeon, J.-M. Hong, S. Fabiano, M. Berggren and T.-W. Kim, *Org. Electron.*, 2020, **78**, 105554.
4 R. B. Salikhov, A. N. Lachinov and R. G. Rakhmeyev, *J. Appl. Phys.*, 2007, **101**, 053706.
5 A. A. Bunakov, A. N. Lachinov and R. B. Salikhov, *Tech. Phys.*, 2003, **48**, 626 (*Zh. Tekh. Fiz.*, 2003, **73**, 104).
6 R. B. Salikhov, A. N. Lachinov and A. A. Bunakov, *Phys. Solid State*, 2007, **49**, 185 (*Fiz. Tverd. Tela*, 2007, **49**, 179).
7 G. Ziyatdinova and H. Budnikov, in *Nanoanalytics: Nanoobjects and Nanotechnologies in Analytical Chemistry*, ed. S. Shtykov, De Gruyter, Berlin, 2018, pp. 223–252.
8 R. Montes, J. Bartrolí, F. Céspedes and M. Baeza, *J. Electroanal. Chem.*, 2014, **733**, 69.
9 E. S. Kobeleva, D. A. Nevostruev, M. N. Uvarov, D. E. Utkin, V. A. Zinoviev, O. A. Gurova, M. S. Kazantzev, K. M. Degtyarenko, A. V. Kulikova and L. V. Kulik, *Russ. Chem. Bull.*, 2021, **70**, 2427.
10 J. Muñoz, R. Montes and M. Baeza, *TrAC, Trends Anal. Chem.*, 2017, **97**, 201.
11 K. Murtada and V. Moreno, *J. Electroanal. Chem.*, 2020, **861**, 113988.
12 M. L. Yola, *Curr. Anal. Chem.*, 2019, **15**, 159.
13 A. A. Taherpour and F. Mousavi, in *Fullerens, Graphenes and Nanotubes: A Pharmaceutical Approach*, ed. A. M. Grumezescu, Elsevier, 2018, pp. 169–225.
14 S. K. Krishnan, E. Singh, P. Singh, M. Meyyappan and H. S. Nalwa, *RSC Adv.*, 2019, **9**, 8778.
15 Q. Zhang, M. Fu, H. Lu, X. Fan, H. Wang, Y. Zhang and H. Wang, *Sens. Actuators, B*, 2019, **296**, 126667.
16 G. Wang, A. Morrin, M. Li, N. Liu and X. Luo, *J. Mater. Chem. B*, 2018, **6**, 4173.
17 A. K. Srivastava, S. S. Upadhyay, C. R. Rawool, N. S. Punde and A. S. Rajpurohit, *Curr. Anal. Chem.*, 2019, **15**, 249.
18 R. A. Zilberg, Yu. B. Teres, L. R. Zagitova, Yu. A. Yarkaeva and T. V. Berestova, *Analitika i kontrol' (Analytics and Control)*, 2021, **25**, 193 (in Russian).
19 R. A. Zil'berg, Yu. A. Yarkaeva, E. I. Maksyutova, A. V. Sidel'nikov and V. N. Maistrenko, *J. Anal. Chem.*, 2017, **72**, 402 (*Zh. Anal. Khim.*, 2017, **72**, 348).
20 R. A. Zil'berg, V. N. Maistrenko, Yu. A. Yarkaeva and D. I. Dubrovskii, *J. Anal. Chem.*, 2019, **74**, 1245 (*Zh. Anal. Khim.*, 2019, **74**, 941).
21 R. A. Zil'berg, Yu. A. Yarkaeva, A. V. Sidel'nikov, V. N. Maistrenko, V. A. Kraikin and N. G. Gileva, *J. Anal. Chem.*, 2016, **71**, 926 (*Zh. Anal. Khim.*, 2016, **71**, 964).
22 V. A. Kraikin, A. A. Fatykhov, N. G. Gileva, A. A. Kravchenko and S. N. Salazkin, *Magn. Reson. Chem.*, 2021, **59**, 61.
23 S. N. Salazkin, V. V. Shaposhnikova, L. N. Machulenko, N. G. Gileva, V. A. Kraikin and A. N. Lachinov, *Polym. Sci., Ser. A*, 2008, **50**, 243 (*Vysokomol. Soedin., Ser. A*, 2008, **50**, 399).
24 N. G. Gileva, V. A. Kraikin, E. A. Sedova, M. S. Lobov, S. I. Kuznetsov and S. N. Salazkin, *Russ. J. Appl. Chem.*, 2005, **78**, 1683 (*Zh. Prikl. Khim.*, 2005, **78**, 1712).
25 R. A. Zilberg, A. V. Sidelnikov, V. N. Maistrenko, Y. A. Yarkaeva, E. M. Khamitov, V. M. Kornilov and E. I. Maksutova, *Electroanalysis*, 2018, **30**, 619.
26 H. Xu, Q. Zheng, P. Yang, J. Liu and L. Jin, *Chin. J. Chem.*, 2011, **29**, 805.
27 A. Lasia, *Electrochemical Impedance Spectroscopy and its Applications*, Springer, New York, 2014.
28 A. J. Bard and L. R. Faulkner, *Electrochemical Methods: Fundamentals and Applications*, 2nd edn., Wiley, New York, 2004.
29 A. R. Tameev, R. G. Rakhmeev, V. R. Nikitenko, R. B. Salikhov, A. A. Bunakov, A. N. Lachinov and A. V. Vannikov, *Phys. Solid State*, 2011, **53**, 195 (*Fiz. Tverd. Tela*, 2011, **53**, 182).
30 L. E. Arvizu-Rodriguez, U. Paramo-García and F. Caballero-Briones, *Mater. Lett.*, 2020, **276**, 128176.
31 C. Smithson, Y. Wu, T. Wigglesworth, S. Gardner, S. Zhu and H.-Y. Nie, *Org. Electron.*, 2014, **15**, 2639.

Received: 30th December 2021; Com. 21/6783